# Solution-processed green-sensitive organic photoconductive device using rhodamine 6G

Takeshi Fukuda, Sho Kimura, Zentaro Honda, and Norihiko Kamata

Department of Functional Materials Science, Saitama University

255 Shimo-Okubo, Sakura-ku, Saitama 338-8570, Japan

Corresponding author: Takeshi Fukuda

Electronic mail: fukuda@fms.saitama-u.ac.jp

Tel and Fax: +81-48-858-3526

Since rhodamine 6G (R6G) has the selective absorption band at the green wavelength regions, the green-sensitive organic photoconductive device was demonstrated using R6G as a photoconductive layer. By optimizing the conductivity of poly(3,4-ethylenedioxythiophene):poly(styrenesulfonate) (PEDOT:PSS) used as the carrier transport layer and the concentration of R6G, the maximum external quantum efficiency of 32.6 % was obtained at the electric field of -34 MV/m. We found that the low-conductivity of the PEDOT:PSS layer was most important factor for the improved device performance. In addition, the signal-to-noise ratio (photocurrent/dark current) was improved by reducing the conductivity of the PEDOT:PSS layer, and the highest value of 60 was achieved.

Keyword: organic photoconductive device, color selectivity, solution process, rhodamine 6G, organic image sensor, green-sensitive photoconductive device

## Introduction

Since organic devices can be fabricated by the solution process [1,2], organic image sensors have been interested for image sensing applications [3-6]. This is because several organic materials have special advantages over inorganic materials, such as the selective absorption band at the visible wavelength region, the high absorption coefficient, and the possibility of the roll-to-roll printing process [7-10]. Nowadays, the organic image sensor was demonstrated in combination with blue-, green-, and red-sensitive organic photoconductive devices [3]. However, the low-fabrication cost is important factor for practical applications of organic devices, and the solution-processed organic photoconductive devices have been investigated [11-13]. Since the multilayer structure is difficult to fabricate by the solution process, the performance of the solution processed organic photoconductive device is lower than those of a multilayer device fabricated by the thermal evaporation process [7,11].

By now, our previous papers demonstrated improved photoconductive characteristics of the solution-processed blue-sensitive organic device by doping silole derivative in the blue-sensitive polymer [13,14]. In addition, Seo et al. reported the green-sensitive organic photoconductive device fabricated by the thermal evaporation process, and the high-photoconductive characteristics have been already realized [7]. These facts indicate the solution-processed green-sensitive organic photoconductive device has been required for the low-cost organic image sensor. However, little is known about the solution-processed green-sensitive organic photoconductive device.

In this paper, we investigated the green-sensitive organic photoconductive device using rhodamine 6G (R6G) with the selective absorption band at the green-wavelength region [15,16]. At first, several kinds of poly(3,4-ethylenedioxythiophene):poly(styrenesulfonate) (PEDOT:PSS) with different conductivities [17-19] were inserted between the indium tin oxide (ITO) layer and the organic photoconductive layer as a carrier transport layer. Then, we also investigated the relationship between the concentration of R6G in poly(9,9-di-n-octylfluorenyl-2,7-diyl) (PFO) and

the photoconductive characteristics of the green-sensitive organic device.

**Experimental**

A glass substrate covered with the patterned ITO-electrode was ultrasonically cleaned using solvent and deionized water. The thickness of the ITO layer was 150 nm. The ITO-coated glass substrate was then treated with ultraviolet ozone for 20 min just before use.

We used 4 kinds of PEDOT:PSS (P VP CH8000, P VP AI 4083, P HC V4, and PH500). All the PEDOT:PSS were purchased from H.C. Stark. The conductivity, the viscosity, the ratio of PEDOT:PSS, and the work function are summarized in Table 1. The PEDOT:PSS solution was spin-coated at the rotation speed of 6000 rpm for 60 sec in the nitrogen atmosphere. However, the rotation speed was changed as 4500 rpm for only the case of P VP Al 4083 due to the lower viscosity compared to other PEDOT:PSS. Then, the sample was annealed at 140 ℃ for 15 min. In addition, R6G (Aldrich) was used as a green-sensitive organic material, and it was dissolved in chloroform with the concentration of 1 wt%. PFO (Aldrich) was then also added into the resulting solution. We varied the doping concentration of R6G in PFO in the range from 10 to 80 wt%.

After passing through a filter with 0.45-μm-diameter holes, the mixed solution was spin-coated at the rotation speed of 1800 rpm for 60 sec in the nitrogen atmosphere. The sample was then annealed at 70 °C for 60 min to remove any residual chloroform. Finally, the Al electrode (100 nm) was thermally evaporated successively on the R6G:PFO layer.

The external quantum efficiency (EQE), defined as the number of output electrons divided by the total number of irradiated photons, was estimated from the measured photocurrent density and the irradiated optical intensity [11]. The current density was measured using a DC voltage current source/monitor (ADCMT, 6241A). In addition, we used the green light-emitting diode (LED) with the center wavelength of 525 nm. The optical intensity of the green LED was 0.7 mW/cm$^2$, and the focus area was almost the same as the device area (3 mm x 3 mm). The photocurrent density was measured while irradiating the green light, and the dark

current density was measured without irradiating the green light. <u>The photocurrent density was calculated as the dark current density subtracted from the measured current density while irradiating the green light.</u> Furthermore, the signal-to-noise ratio (S/N) was estimated as the photocurrent density divided by the dark current density. The absorption spectra of R6G and PFO neat films were measured using a double-beam ultraviolet/visible spectrophotometer (V-650, JASCO). The absorption coefficient was calculated from the transmittance and the thickness of the organic layer measured using a surface profile meter (Alpha-Step IQ, KLA Tencor). <u>In addition, highest occupied molecular orbital (HOMO) and lowest unoccupied molecular orbital (LUMO) levels were determined by photoelectron spectroscopy (Riken Keiki, AC-3) and the absorption spectrum.</u>

**Results and Discussion**

The measured thicknesses of PEDOT:PSS layers were 50, 25, 70, and 25 nm for P VP CH8000, P VP AI 4083, P HC V4, and PH500, respectively. In addition, the thickness of the R6G layer was 130 nm at the concentration of 20 wt%. Figure 1 shows the absorption spectra of R6G and PFO neat films. As clearly shown in Fig. 1, the R6G neat film had a selective absorption band at the green wavelength region. The maximum absorption coefficient was $3.1 \times 10^5$ cm$^{-1}$ at 558 nm, and this value was high enough to absorb the incident light. On the other hand, the PFO neat film had little absorption coefficient at the visible wavelength region. Therefore, most of the incident light was absorbed by R6G while irradiating the green light.

Figures 2(a) and (b) show the photocurrent density while irradiating the green light and the <u>S/N</u> of the organic photoconductive devices with different kinds of PEDOT:PSS, respectively. The concentration of R6G:PFO was fixed 20 wt%, and the structure of the reference device was ITO/R6G:PFO/Al (without PEDOT:PSS).

The larger photocurrent densities were obtained compared to the reference device without the PEDOT:PSS layer when P HC V4 and PH500 were used as the carrier transport layers due to the high conductivity [18,19]. Since work functions of all the PEDOT:PSS layers were almost same, this result indicates the photo-induced carrier efficiently

moves to the electrode side. In addition, the dark current density decreased with decreasing conductivity of the PEDOT:PSS layer for both sides of positive and negative electric fields. This is because the photo-induced carriers efficiently transport in the PEDOT:PSS layer, and the high current density was obtained when the conductivity of PEDOT:PSS was high. Especially, the lowest dark current density by applying the negative electric field was realized when P VP CH 8000 was used.

Figure 2(b) shows the S/N of the fabricated organic photoconductive devices with different PEDOT:PSS layers. The high-S/N is required for image sensing applications, and it is realized by the reduced dark current density [11]. The highest S/N was realized when P VP CH8000 with the lowest conductivity was used. The maximum S/N was 60 at the electric field of 32 MV/m.

The energy diagram of the fabricated organic photoconductive device is shown in Fig. 3. The work function of the PEDOT:PSS layer (5.0 eV) was placed between the HOMO level of R6G (5.35 eV) and the that of the ITO layer (4.7 eV).

Therefore, the large dark current density was observed at the positive bias voltage due to the efficient carrier injection from the ITO layer to the PEDOT:PSS layer [20,21]. On the other hand, the LUMO level of the R6G layer was 3.28 eV, and the large energy gap was formed at the PEDOT:PSS/R6G interface to inject the hole while applying the negative bias voltage. As a result, the low dark current density was realized while applying the negative bias voltage, as shown in Fig. 2(b).

For further improved photoconductive characteristics of the green-sensitive device using R6G, we investigated the concentration dependence of the R6G:PFO layer on the device performances. Here, P VP CH8000 was used as the carrier transport layer, and P VP CH8000 showed the highest photocurrent density (Fig 2). Figures 4(a) and (b) show the photocurrent and the dark current densities of the organic photoconductive devices with different concentrations of R6G:PFO. The internal field was formed by irradiating the green light, and the photocurrent density-voltage characteristic shifts toward the positive electric

field condition when the concentration of R6G was less than 30 %. Both the photocurrent and the dark current densities tended to increase with increasing concentration of R6G. Since the absorption coefficient of the R6G:PFO layer increases with increasing concentration of R6G, the large amount of photo-induced carriers are generated in the organic layer. In addition, the HOMO/LUMO levels of R6G act as the carrier transport pass from the photoconductive layer to the electrode. Therefore, the large current density was observed at the high concentration condition. However, the increase trend of the dark current density was suppressed up to 30 % while applying the negative bias voltage even though the photocurrent density continuously increased with increasing concentration of R6G. The most likely cause is that the aggregated R6G causes the increased dark current density; therefore, the low dark current density was suppressed at the low concentration region less than 30 %.

Figures 5(a) and (b) show the EQE and the S/N of the organic photoconductive devices with different concentration of R6G ranged from 10 to 30 wt%. Here, the current density-voltage characteristics provided only at the concentration of less than 30 %

. The EQE increased with increasing concentration of R6G in PFO due to the high photocurrent density, as shown in Fig. 4(a). The highest EQE of 32.6 % was realized at -34 MV/m. In addition, the S/N also increased with increased concentration of R6G while applying the negative bias voltage. The S/Ns were almost same for all the devices when the positive bias voltage was applied due to the large dark current density, as shown in Fig. 3(b).

**Conclusion**

The EQE and S/N were improved by optimizing the conductivity of PEDOT:PSS layer and the concentration of R6G. The low-conductivity of the PEDOT:PSS layer is important factor to reduce the dark current density, resulting in the high S/N. The maximum EQE of 32.6 % was achieved by optimizing the concentration of R6G.

**References**

[1] Krebs, F.C., (2009). Sol. Energy Mater. Sol. Cells, 93, 394.

[2] Fukuda, T., Asaki, H., Asano, T., Takagi, K., Honda, Z., Kamata, N., Ju, J., & Yamagata, Y., (2011). Thin Solid Films, 520, 600.

[3] Aihara, S., Seo, H., Namba, M., Watabe, T., Ohtake, H., Kubota, M., Egami, N., Hiramatsu, T., Matsuda, T., Furuta, M., Nitta, H., & Hirao, T., (2009). IEEE Trans. Electron. Dev., 56, 2570.

[4] Lamprecht, B., Thünauer, R., Köstler, S., Jakopic, G., Leising, G., & Krenn, J.R., (2008). Phys. Stat. Sol. (RRL), 2, 178.

[5] Street, R.A., Graham, J., Popovic, Z.D., Hor, A., Ready, S., & Ho, J., (2002). J. Non-Cryst. Sol., 299-302, 1240.

[6] Fukuda, T., Komoriya, M., Mori, R., Honda, Z., Takahashi, K., & Kamata, N., (2009). Mol. Cryst. Liq. Cryst., 504, 212.

[7] Seo, H., Aihara, S., Watabe, T., Ohtake, H., Kubota, M., & Egami, N., (2007). Jpn. J. Appl. Phys., 49, L1240.

[8] Yang, Y., Omi, S., Goto, R., Yahiro, M., Era, M., Watanabe, H., Oki, Y., (2011). Org. Electron., 12, 405.

[9] Higashi, Y., Kim, K.-S., Jeon, H.-G., & Ichikawa, M., (2010). J. Appl. Phys., 108, 034502.

[10] Fukuda, T., Kobayashi, R., Kamata, N., Airaha, S., Seo, H., Hatano, K., Terunuma, D., (2010). Jpn. J. Appl. Phys., 49, 01AC05.

[11] Fukuda, T., Komoriya, M., Kobayashi, R., Ishimaru, Y., Kamata, N., (2009). Jpn. J. Appl. Phys., 48, 04C162.

[12] Fukuda, T., Suzuki, T., Kobayashi, R., Honda, Z., & Kamata, N., (2009). Thin Solid Films, 518, 575.

[13] Kobayashi, R., Fukuda, T., Suzuki, Y., Hatano, K., Kamata, N., Aihara, S., Seo, H., & Terunuma, D., (2010). Mol. Cryst. Liq. Cryst., 519, 206.

[14] Fukuda, T., Kobayashi, R., Kamata, N., Aihara, S., Seo, H., Hatano, K., & Terunuma, D., (2010). Jpn. J. Appl. Phys., 49, 01AC05.

[15] Vogel, R., Meredith, P., Harvey, M.D., & Rubinsztein-Dunlop, H., (2004). Spectrochim. Acta A, Mol. Biomol. Spectrosc., 60, 245.

[16] Dolan, G., Goldschmidt, C.R., (1976). Chem. Phys. Lett., 39, 320.

[17] Weijtens, C.H.L., Elsbergen, V.van, Kok, M.M.de, & Winter, S.H.P.M.de, (2005). Org. Electron., 6, 97.

[18] Zhou, Y., Zhang, F., Tvingstedt, K., Barrau, S.,

Li, F., Tian, W., & Inganäs, O., (2008). Appl. Phys. Lett., 92, 233308.

[19] Kajii, H., Ohmori, Y., Maki, H., Sekimoto, Y., Shigeno, Y., Takehara, N., & Nakagawa, H., (2008). Jpn. J. Appl. Phys., 47, 460.

[20] Choulis, S.A., Choong, V.E., Patwardhan, A., Mathai, M.K., & So, F., (2006). Adv. Funct. Mater., 16, 1075.

[21] Kok, M.M.de, Buechel, M., Vulto, S.I.E., Weijer, P.van de, Meulenkamp, A., Winter, S.H.P. M. de, Mank, A.J.G., Vorstenbosch, H.J.M., Weijtens, C.H.L., Elsbergen, V. van, (2004). Phys. Stat. Sol. (a), 201, 1342.

**Table and Figure Captions**
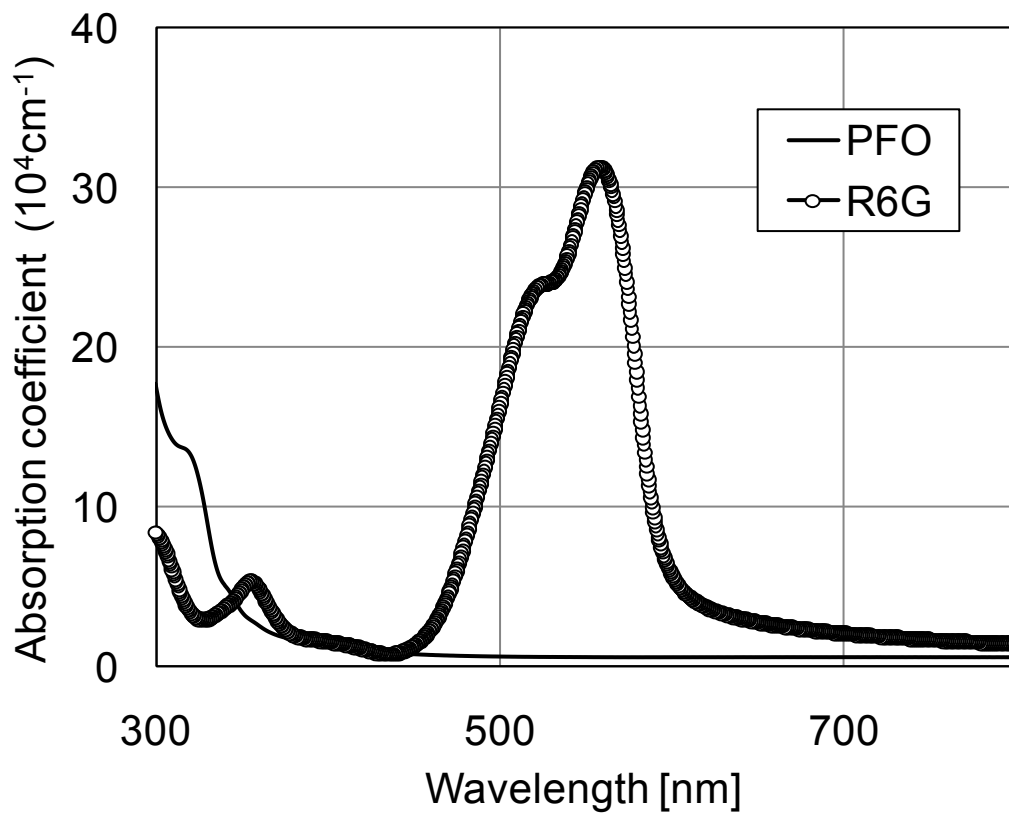
Table 1 Characteristics of used PEDOT:PSS.

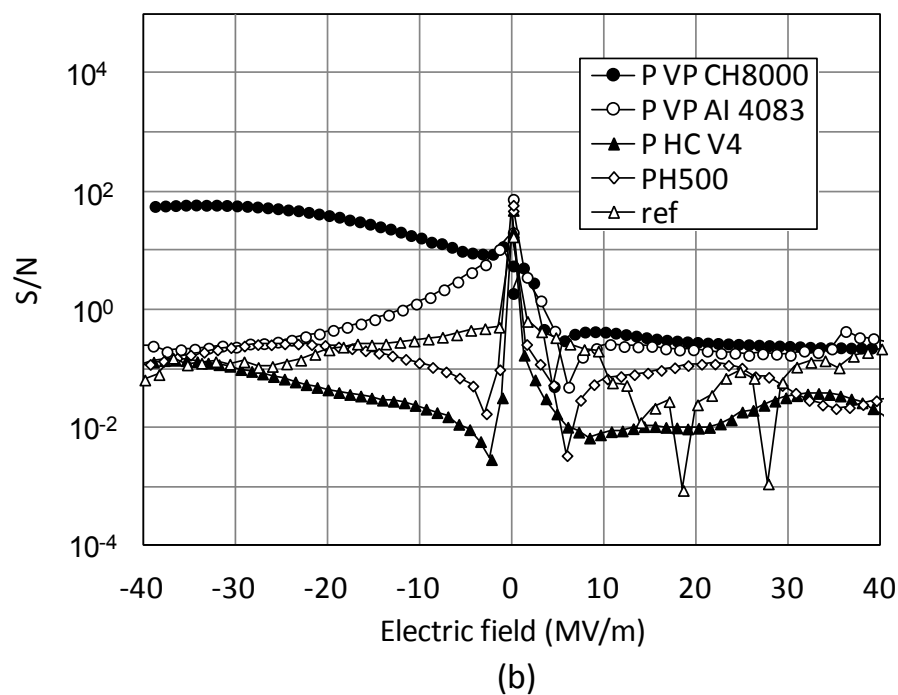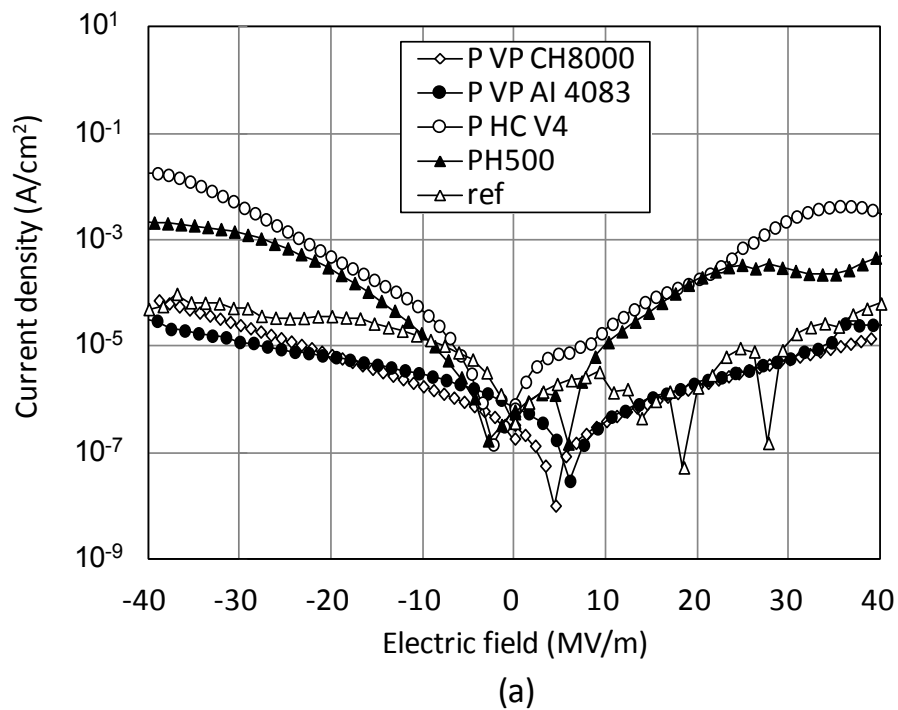Fig. 1 Absorption spectra of R6G and PFO neat films.

Fig. 2 (a) Photocurrent density while irradiating the green light and (b) the S/N of the organic photoconductive devices with different PEDOT:PSS layers.

Fig. 3 Energy diagram of the organic photoconductive device.

Fig. 4 (a) Photocurrent density while irradiating the green light and (b) the dark current density of organic photoconductive devices with different concentrations of R6G as a function of the electric field.

Fig. 5 (a) EQE and (b) the S/N of the green-sensitive organic photoconductive devices with different concentrations of R6G ranged from 10 to 30 wt%.

Table 1 Characteristics of used PEDOT:PSS.

| | Conductivity (S/cm) | Viscosity (mPa·s) | Ratio of PEDT:PSS | Work function (eV) |
|---|---|---|---|---|
| P VP CH8000 | $3.3\times10^{-6}$- $1.0\times10^{-5}$ | 9～20 | 1 : 20 | 5.0～5.2 |
| P VP AI 4083 | $2.0\mathrm{x}10^{-4}$- $2.0\mathrm{x}10^{-3}$ | 5～12 | 1 : 6 | 5.0～5.2 |
| P HC V4 | $2.0\times10^{2}$- $5.0\times10^{2}$ | 100～350 | 1 : 2.5 | 5.0～5.1 |
| PH500 | $3.0\times10^{2}$- $5.0\times10^{2}$ | 8～25 | 1 : 2.5 | 5.0～5.1 |

Fig. 1 Absorption spectra of R6G and PFO neat films.

(a)



(b)

Fig. 2 (a) Photocurrent density while irradiating the green light and (b) the S/N of the organic

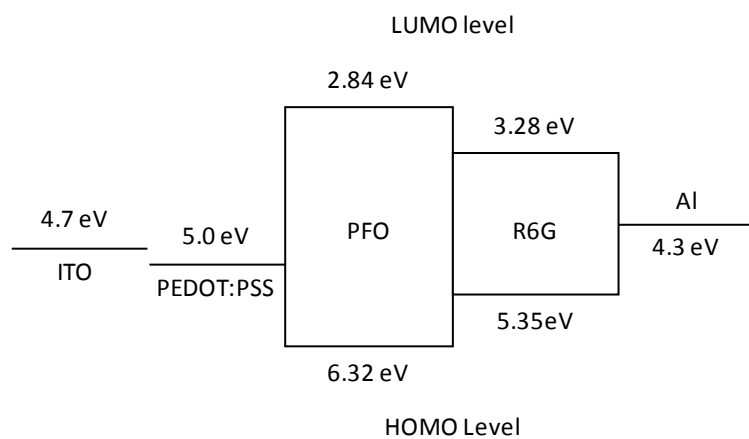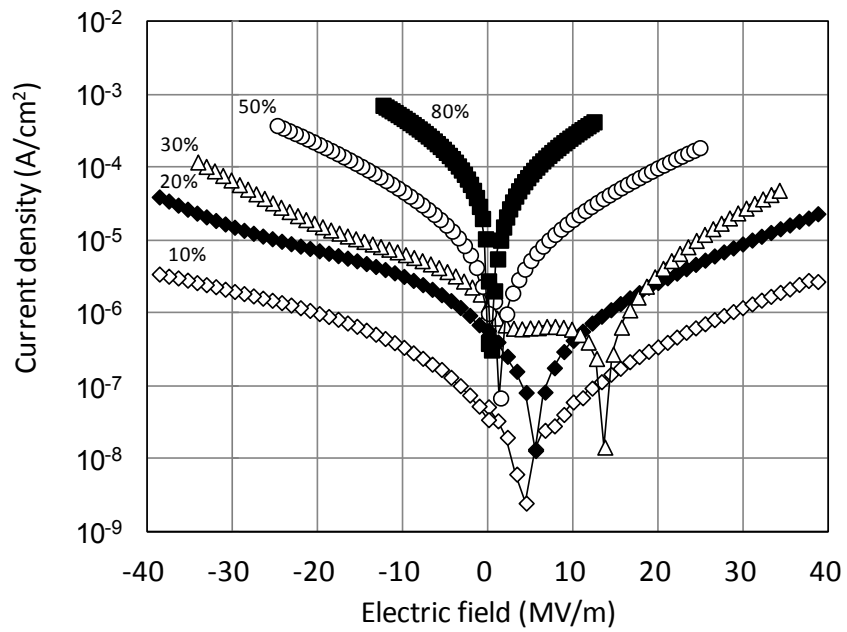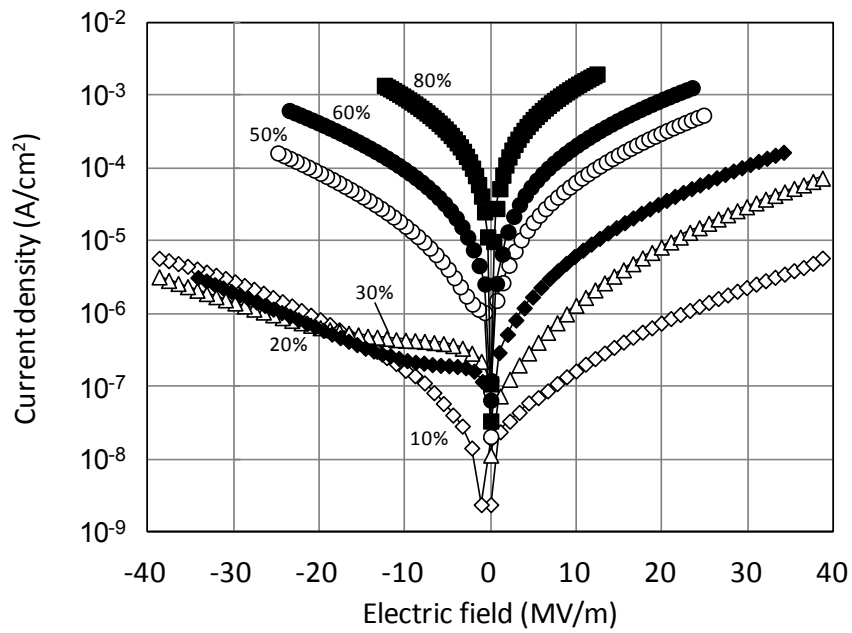photoconductive devices with different PEDOT:PSS layers.

LUMO level

2.84 eV

3.28 eV

4.7 eV          5.0 eV              PFO        R6G        Al

ITO                                                      4.3 eV

PEDOT:PSS                                   5.35eV

6.32 eV

HOMO Level
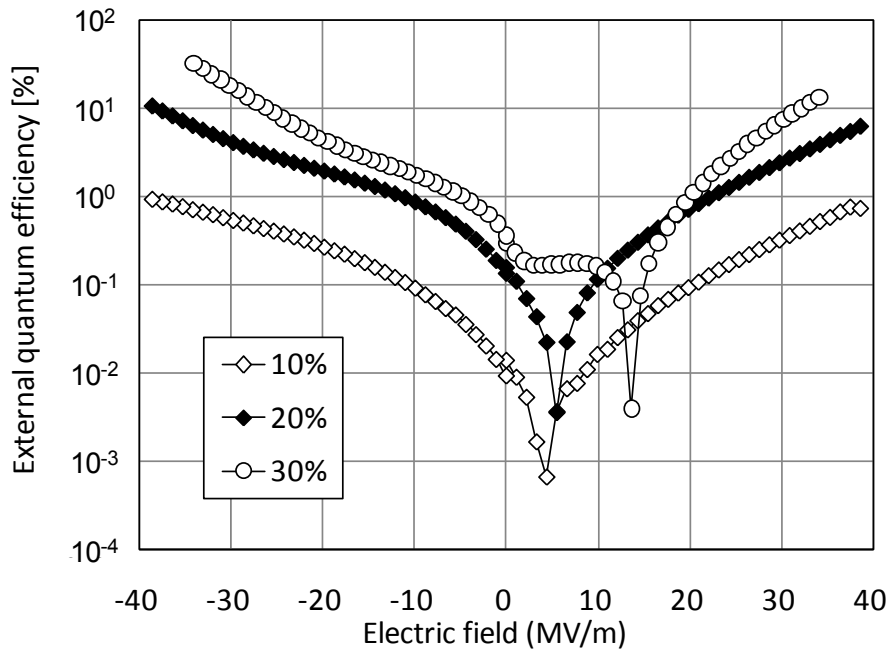
Fig. 3 Energy diagram of the organic photoconductive device.
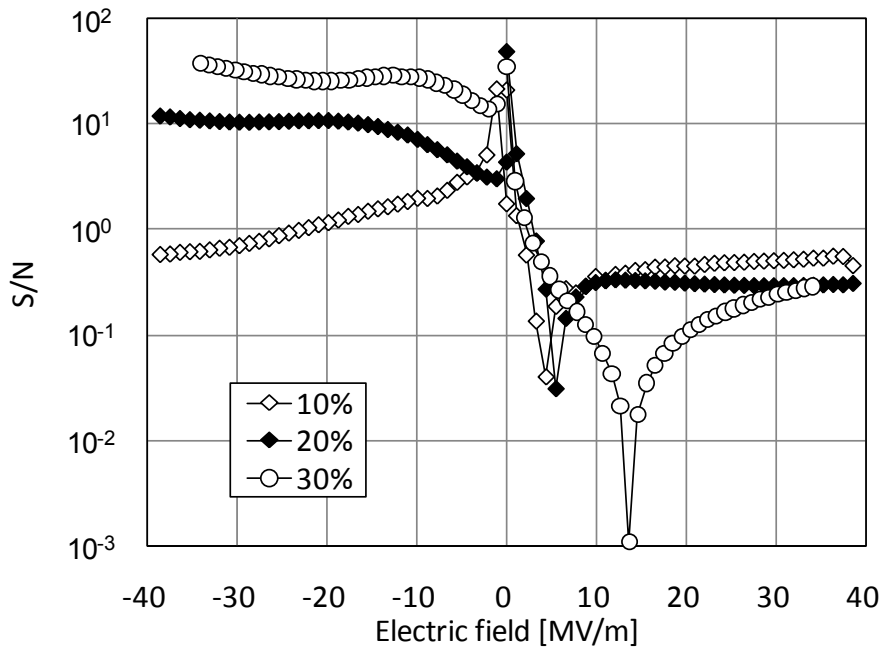
Fig. 4 (a) Photocurrent density while irradiating the green light and (b) the dark current density of organic photoconductive devices with different concentrations of R6G as a function of the electric field.

Fig. 5 (a) EQE and (b) the S/N of the green-sensitive organic photoconductive devices with different

concentrations of R6G ranged from 10 to 30 wt%.